Published in final edited form as:

Circulation. 2022 May 24; 145(21): 1609–1624. doi:10.1161/CIRCULATIONAHA.120.049261.

Progressive Reduction in Right Ventricular Contractile Function Due to Altered Actin Expression in an Aging Mouse Model of Arrhythmogenic Cardiomyopathy

Emmanuel M. Camors, PhD[1,2], **Alyson H. Roth, BS**[1,2], **Joseph R. Alef, MS**[1,2], **Ryan D. Sullivan, DVM**[3], **Jason N. Johnson, MD**[1,2,4], **Enkhsaikhan Purevjav, MD, PhD**[1,2], **Jeffrey A. Towbin, MD**[1,2,4]

[1]Heart Institute, Department of Pediatrics, University of Tennessee Health Science Center, Memphis, TN

[2]Children's Foundation Research Institute, Le Bonheur Children's Hospital, Memphis, TN

[3]Department of Internal Medicine, University of Arizona College of Medicine, Phoenix, AR

[4]Pediatric Cardiology, St. Jude Children's Research Hospital, Memphis, TN.

Abstract

Background: Arrhythmogenic cardiomyopathy (ACM) is an inherited genetic disorder of desmosomal dysfunction, and plakophilin-2 (PKP2) has been reported to be the most common disease-causing gene when mutation-positive. In the early "concealed" phase, the ACM heart is at high risk of sudden cardiac death before cardiac remodeling occurs due to mistargeted ion channels and altered Ca^{2+} handling. However, the results of pathogenic PKP2 variants on myocyte contraction in ACM pathogenesis remain unknown.

Methods: We studied the outcomes of a human truncating variant of PKP2 on myocyte contraction using a novel knock-in mouse model with insertion of thymidine in exon 5 of *Pkp2*, which mimics a familial case of ACM (PKP2-L404fsX5). We used serial echocardiography, electrocardiography, blood pressure measurements, histology, cardiomyocyte contraction, intracellular calcium measurements, and gene and protein expression studies.

Results: Serial echocardiography of Pkp2 heterozygous (Pkp2-Het) mice revealed progressive failure of the right ventricle (RV) in animals older than three months of age. By contrast, left ventricular (LV) function remained normal. Electrocardiograms of six-month-old anesthetized Pkp2-Het mice showed normal baseline heart rates and QRS complexes. Cardiac responses to β-adrenergic agonist isoproterenol (2 $mg.kg^{-1}$) plus caffeine (120 $mg.kg^{-1}$) were also normal. However, adrenergic stimulation enhanced the susceptibility of Pkp2-Het hearts to tachyarrhythmia and sudden cardiac death. Histologic staining showed no significant fibrosis or adipocyte infiltration in the RVs and LVs of six- and twelve-month-old Pkp2-Het hearts. Contractility assessment of isolated myocytes demonstrated progressively reduced Pkp2-Het RV

Address for Correspondence: Jeffrey A. Towbin, M.D., The Heart Institute, Le Bonheur Children's Hospital, 49 N. Dunlap St, FOB Room 344, Memphis, TN 38103, USA., Phone: (901) 287-6819., Fax: (901) 287-5970., jtowbin1@uthsc.edu.

Disclosures

None.

cardiomyocyte function consistent with RV failure measured by echocardiography. However, aging Pkp2-Het and control RV myocytes loaded with intracellular Ca^{2+} indicator Fura-2 showed comparable Ca^{2+} transients. Western blotting of Pkp2-RV homogenates revealed a 40% decrease in actin, while actin immunoprecipitation followed by a 2, 4-dinitrophenylhydrazine staining showed doubled oxidation level. This correlated with a 39% increase in troponin-I phosphorylation. In contrast, Pkp2-Het LV myocytes had normal contraction, actin expression and oxidation, and troponin-I phosphorylation. Finally, Western blotting of cardiac biopsies revealed actin expression was 40% decreased in RVs of end-stage ACM patients.

Conclusions: During the early "concealed" phase of ACM, reduced actin expression drives loss of RV myocyte contraction, contributing to progressive RV dysfunction.

Keywords

Arrhythmogenic cardiomyopathy; Plakophilin-2; Aging; Sarcomere contraction

Introduction

Arrhythmogenic cardiomyopathies (ACMs) are hereditary genetic disorders that originate, for most cases, from pathogenic variants of desmosomal genes[1–4]. The impairment of desmosome organization weakens cell-to-cell adhesion and activates stress/stretch-induced apoptotic pathways, causing the progressive replacement of cardiac myocytes by fibrosis and fat infiltration[1,4]. The clinical picture of ACM depends on the stage of the disease. In the early "concealed" phase, ACM hearts exhibit a risk of life-threatening ventricular tachyarrhythmias, palpitations, arrhythmic syncope, and sudden cardiac death (SCD) in the absence of structural remodeling. In the "electrical" phase, fibrosis and adipose tissue have progressively infiltrated the myocardium, most commonly the right ventricle (RV), increasing the risk of SCD. In the late stage, as the fibrofatty infiltration has affected both ventricles, ACM hearts exhibit biventricular chamber dilation and the mechanical characteristics of a failing heart[1–4].

Desmosomes are comprised of three types of proteins: 1) transmembrane cadherins desmocollin-2 and desmoglein-2, which facilitate cell-to-cell adhesion in the extracellular core region; 2) armadillo proteins plakoglobin and plakophilin-2 (PKP2), which interact with both cadherins; and 3) the cytoskeleton adaptor desmoplakin that connects the desmosome to the intermediate filament desmin[5]. Pathogenic variants of the *PKP2* gene account for over 40% of desmosome-associated ACM cases[6]. In the clinic, they lead to a right ventricular-dominant form of ACM, and they often originate from nucleotide(s) insertion/deletion in the coding sequence of *PKP2* causing a frameshift and an early stop[1,2]. Recent mouse models have demonstrated additional roles of PKP2 in forming gap junctions, targeting Na^{+} channels to intercalated disks, and regulating Ca^{2+} handling proteins[7–9]. Nonetheless, how *PKP2* pathogenic variants affect ventricular and cardiac myocyte contraction remains largely undefined. Here, we created a novel knock-in mouse model of ACM based on insertion of a thymidine into a mouse *Pkp2* coding sequence (c.1086InsT). The thymidine insertion reproduces a human variant, *PKP2-c.1212InsT* (Figure 1A, Clinvar: VCV000045015.9). This variant, identified in three different pedigrees from ACM cases, associates with RV-only dysfunction, minor to major structural abnormalities, arrhythmias,

sustained ventricular tachycardia, and episodes of SCD[6,10,11]. In this study, we compared the RV versus left ventricle (LV) properties of three-, six-, and twelve-month-old sedentary mice and evaluated the impact of the *Pkp2* variant on ventricular remodeling, myocyte contraction, Ca^{2+} handling, and protein expression. Overall, the *Pkp2-c.1086InsT* variant was found to lead to a progressive ACM phenotype characterized by reduced actin expression and decreased myocyte contraction capacity in the RV and enhanced LV sensitivity to life-threatening arrhythmias.

Methods

Extended methods are available in the online supplemental material. The data, methods, and study materials used to conduct the research will be available from the corresponding author upon reasonable request.

General Information

The University of Tennessee Health Science Center Institutional Animal Care and Use Committee (IACUC) approved all protocols and animal procedures used for this study. Both female (N= 32) and male (N= 70) mice were used.

Human Hearts

Human control (N= 3) and ACM (N= 4) biopsies were collected from de-identified autopsy specimens. ACM samples were obtained from patients with end-stage ACM disorder, while Control samples were obtained from patients who exhibited no clinical or pathological evidence of cardiac disease or dysfunction. There was no genetic analysis of the ACM patients. This study was approved by the Le Bonheur Children's Hospital Institutional Review Board committee. Written informed consent was obtained from all participating subjects and/or their guardians.

Generation of the Pkp2-L362fsX21 Knock-in Mouse Model

The Pkp2-L362fsX21 knock-in mouse model was generated using a gene-targeting knock-in approach as described previously (Figure S1)[12].

Echocardiographic Assessment of Cardiac Function

Serial echocardiography was performed every six weeks for up to six months followed by final imaging at one year. Mice (N= 5–7 animals per group) were anesthetized in an induction chamber by 5% isoflurane mixed with 0.8–1 L/min oxygen and maintained in an anesthetized state by 1–2% isoflurane. The animals were then placed in a supine position atop a heating pad with ECG leads. Body temperature was continuously monitored and maintained at 37±0.2 °C throughout the recordings. Transthoracic echocardiography (parasternal short axis and apical four chamber transections) was performed at mid-papillary level using a 30 MHz probe (MS400) connected to a Vivo 2100 system (Visual Sonic, Toronto, ON, Canada). Tricuspid annular plane systolic excursion (TAPSE) was measured in the lateral tricuspid valve annulus from the apical 4-chamber view using M-mode. Cardiac assessments were obtained and analyzed by an operator blinded to the mouse groups using VivoLab 2.1 software (Visual Sonic).

ECG Recordings

Surface ECGs were recorded in slightly anesthetized (1–2% isoflurane) six-month-old mice (N= 6–7 mice per group) using needle ECG electrodes placed under the skin in an equivalent of the lead II configuration. Activation of the sympathetic pathway was elicited by the intraperitoneal injection of an isoproterenol (2 $mg.kg^{-1}$ body weight) and caffeine (120 $mg.kg^{-1}$ body weight) cocktail[13]. Arrhythmic events were segregated by duration between non-sustained (≤5 seconds) and sustained (>5 seconds) arrhythmias.

Mouse Ventricular Myocyte Isolation

Mice (N= 5–6 animals per age per group) received an intraperitoneal injection of 57.2 units/g heparin five to ten minutes prior to euthanasia to prevent blood coagulation and cardiac ischemia during perfusion. Next, the mice were deeply anesthetized in an induction chamber by isoflurane vapor and sacrificed by cervical dislocation. Mouse hearts were quickly excised for mounting on a Langendorff perfusion system via cannulation of the aorta. Hearts were retro-perfused at 37 °C in basic Tyrode's solution (containing in mM: 140 NaCl, 5.4 KCl, 1.2 NaH_2PO_4, 1 $MgCl_2$, 10 Glucose, 8 Taurine, and 10 HEPES, pH 7.4 with NaOH), bubbled with 95% O2–5% CO2 mix, and digested by 200 units/mL Collagenase type II enzyme (Worthington Biochemical Co., Lakewood, NJ) in 20 μM $CaCl_2$ Tyrode's solution. After digestion, left and right ventricular free walls (LVFWs and RVFWs, respectively) were carefully dissected, and cells were isolated by mechanical disruption. Collagenase activity was stopped by 1% BSA in 20 μM $CaCl_2$ Tyrode's solution. The freshly isolated myocytes were sequentially washed in increasing $CaCl_2$ concentrations and finally stored at room temperature (RT) in 1 mM $CaCl_2$ Tyrode's solution. Cells were considered alive for up to six hours after the isolation.

Sarcomere Shortening and Intracellular Calcium Measurements

Cardiomyocyte contractions and intracellular Ca^{2+} transients were recorded at RT under constant superfusion of 1.8 mM $CaCl_2$ Tyrode's solution using an IonOptix Calcium and Contractility Complete System (IonOptix, Westwood, MA). Freshly isolated myocytes were visualized using a 40 X/0.95 N.A. air-dry objective (Olympus, Center Valley, PA) mounted on an AE31 fluorescence microscope (Motic, Richmond, BC, Canada). The cells were field stimulated from 0.5 Hz to 3 Hz by a MyoPacer-EP stimulator (IonOptix). Cardiomyocyte contractions were measured as sarcomere shortenings and recorded by a Myocam-S camera (IonOptix). Intracellular Ca^{2+} concentrations were estimated in myocytes loaded for thirty minutes (RT) with Fura-2, AM (3 μM with 0.04% Pluronic F-127, Molecular Probes, Eugene, OR) followed by a thirty-minute wash. Intracellular Ca^{2+} concentrations were determined by the ratio of Fura-2 emission (510±40 nm band-pass filter) from successive excitations at 340 nm (Ca^{2+} bound) and 380 nm (Ca^{2+} free) (HyperSwitch, IonOptix) by a 60 Hz Xenon lamp (CAIRN). Background noise was determined at 340 nm and 380 nm in a cell-free area nearby the measured cardiomyocyte and subtracted from cellular signals (Figure S2). Sarcoplasmic reticulum Ca^{2+} release was elicited by rapid perfusion of 10 mM caffeine. The β-adrenergic pathway was activated by perfusion of myocytes with 100 nM isoproterenol. Cardiomyocyte contractions and intracellular Ca^{2+} concentrations were recorded at a sampling rate of 250 Hz and analyzed by an operator blinded to the

mouse groups. Recordings and their analysis were performed using IonWizard 6 software (IonOptix).

Statistics

Data, presented as means ± standard error of the mean, were analyzed using unpaired Student's *t* test for two group comparisons and analysis of variance (ANOVA) followed by Bonferroni correction for multiple group comparisons using SPSS (version 26.0, IBM, Armonk, NY). Cardiac myocyte contraction and Ca^{2+} handling properties were analyzed using nested t-tests to uncover potential clustering within animals from the same group. *P* values were considered significant at $P<0.05$. Graphs were prepared using Prism 9.0 software (GraphPad, San Diego, CA).

Results

Pkp2-L362fsX21 truncation prevents the development of homozygous mice

The Pkp2-L362fsX21 global knock-in mouse model was generated by insertion of a thymidine in the mouse *Pkp2* gene at position c.1086 to uncover the outcomes of the human *PKP2-c.1212InsT* pathogenic variant[6,10,11] (Figure 1A and Figure S1). Heterozygous Pkp2-L362fsX21 knock-in mice (Pkp2-Het) were healthy, fertile, and exhibited a normal lifespan for up to two years. Nonetheless, inheritance analysis of Pkp2-Het mating revealed an absence of newborn animals homozygous for the mutation. The Mendelian distribution of offspring from Pkp2-Het females in gestation revealed early lethality of homozygous embryos during mid-development (embryonic day 13.5- Figure S3), similar to recently published Pkp2 knock-out models[14–16]. To explain the absence of newborn homozygous mice, we hypothesized Pkp2-c.1086InsT mRNA was recognized as nonfunctional and degraded during translation following nonsense-mediated mRNA decay[17]. Total mRNAs were extracted from the LVFWs and RVFWs of six-month-old Pkp2-Het and WT mice. RT-qPCR revealed a 50% decrease in Pkp2 mRNA abundance in both ventricles of the mutant heart (Figure 1B). The sequencing of individual Pkp2 transcripts[18] further showed only 6 to 11% of Pkp2 mRNAs expressed in ventricles carried the c.1086InsT mutation (Figure S4). Accordingly, (WT) PKP2 protein expression was 50% lower in the Pkp2-Het heart than in the WT heart, while the truncated L362fsX21 isoform (~40 kDa) remained undetectable (Figure 1C and Figure S5). Immunocytochemistry on freshly isolated myocytes from RVFWs showed (WT) PKP2 protein was typically present in the intercalated disks of mutant myocytes (Figure 1D). Altogether, these data demonstrate the absence of mutant Pkp2 mRNAs in the L362fsX21 knock-in mouse heart, similar to nonsense *PKP2* variants identified in human ACM[19].

Pkp2 haploinsufficiency reproduces the right-dominant form of the ACM phenotype

Previous studies implicated PKP2 in embryogenesis[16] as a regulator of Na^+ channels[7] and intracellular Ca^{2+} handling[9]. Nonetheless, the effect of Pkp2 haploinsufficiency on cardiac contraction remains unclear[8]. Therefore, we evaluated the cardiac parameters of aging sedentary mice by serial transthoracic echocardiography. We performed imaging on six-week-old mice, followed by six-week re-evaluations for up to one year. During their first year of life, compared to WT littermates, Pkp2-Het mice exhibited normal LV

function (Figure 1E and Table S3). At twelve months old, LV end diastolic and systolic dimensions and fractional shortening were comparable between Pkp2-Het and age-matched WT hearts (Figure 1F). Similarly, LV ejection fraction and mass were normal, revealing no dilation or hypertrophy of the Pkp2-Het heart. Finally, diastolic and systolic tail blood pressures of six-month-old conscious Pkp2-Het mice were normal (Figure 1G). By contrast, echocardiography revealed progressively declining RV function in Pkp2-Het mice (Figures 2A and 2B and Table S4). At three months of age, RV contraction was the same among mutant and WT mice. At six months of age, RV contraction was 29% lower in mutant RVs than in age-matched WT RVs ($P<0.05$). By one year old, Pkp2-Het RV contraction was 42% lower ($P<0.05$). Notably, we measured a 35% decrease in TAPSE in six-month-old Pkp2-Het hearts compared to that in age-matched WT hearts (0.155±0.02 vs. 0.238±0.01 mm in Pkp2-Het and WT hearts, respectively, $P<0.05$). The late-onset, slow progression of RV-only dysfunction mimicked the clinical picture of non-athletic human ACM cases carrying nonsense *PKP2* pathogenic variants[20,21]. Therefore, to further uncover the origins of RV dysfunction in mutant mice, we tested two hypotheses: 1) the contractile capacity of RV cardiomyocytes progressively declines with aging, and 2) non-excitable cells/tissue (e.g., fibrosis, liposis) increasingly infiltrate the RV.

Progressive reduction in RV myocyte contraction during aging of sedentary Pkp2-Het mice

To test the potential role of RV cardiomyocytes in disease-onset, we determined the force-pacing frequency relationship of isolated myocytes during field stimulation. We recorded sarcomere shortening of myocytes isolated from the LVFW and RVFW of three-, six-, and twelve-month-old mice. We paced myocytes from 0.5 to 3 Hz at RT under constant perfusion of 1.8 mM $CaCl_2$ Tyrode's solution (Figures S6 and S7). In these conditions, all myocytes responded to increased pacing frequencies. However, sarcomere shortening of Pkp2-Het RVFW cells continuously declined with aging. For example, the shortening of twelve-month-old Pkp2-Het RVFW cardiomyocytes paced at 3 Hz was 31% ($P<0.001$) lower than that of age-matched WT myocytes (Figures 2C and 2D, and Table 1). The contraction and relaxation velocities of mutant cells were 34% ($P<0.01$) and 37% ($P<0.01$) lower, respectively, than those of WT cells. As shown in Figure 2E, the reduction in shortening in individual RVFW myocytes correlated with the timing of RV dysfunction in Pkp2-Het hearts. Indeed, the more the mouse aged, the more RVFW myocyte sarcomere shortening decreased and impeded RV function. In contrast, the contraction of Pkp2-Het LVFW myocytes was preserved with aging (Figures 2C and 2E, and Table 1). Next, we tested whether LVFW and RVFW myocytes exhibited physiological differences in contraction in WT and Pkp2-Het mouse hearts. Compared with LVFW myocytes, RVFW myocytes exhibited a tendency for decreased shortening in WT hearts. The sarcomere shortening of twelve-month-old RVFW myocytes paced at 3 Hz was 8% lower than that of LVFW myocytes (P=N.S.), and contraction velocity was 10% lower (P=N.S.). In Pkp2-Het hearts, regional disparities were exacerbated. The contraction amplitude of twelve-month-old RVFW myocytes paced at 3 Hz was 35% lower than that of age-matched LVFW myocytes ($P<0.001$), and contraction velocity was 40% lower ($P<0.001$) (Table 1).

Since myocyte contraction depends on intracellular Ca^{2+} homeostasis, we tested whether intracellular Ca^{2+} handling contributed to Pkp2-Het RV myocyte dysfunction[9,22,23]. We

loaded freshly isolated RVFW myocytes with the intracellular Ca^{2+} indicator, Fura-2, AM, and paced the cells at 1 Hz at RT in 1.8 mM Ca^{2+} Tyrode's solution (Figure S8). At steady state, Pkp2-Het RVFW myocytes exhibited Ca^{2+} transient properties comparable to those of age-matched control RVFW myocytes, i.e., similar diastolic Ca^{2+} concentrations, Ca^{2+} transient amplitudes, time to peak Ca^{2+} release, and time of Ca^{2+} decline (Figures 2F and 2G, and Table 2). We also measured the Ca^{2+} content of the sarcoplasmic reticulum in post-paced myocytes activated by rapid perfusion of 10 mM caffeine[24], and we found comparable SR Ca^{2+} loads between both groups of cells (Figure 2H). Identical Ca^{2+} decay times of caffeine-induced Ca^{2+} transients also suggested unaltered sodium-calcium exchanger (NCX-1) function[25]. Next, we compared the Ca^{2+} transient characteristics between RVFW and LVFW myocytes. We observed significantly reduced Ca^{2+} transient amplitudes, faster Ca^{2+} release, and slower Ca^{2+} decay in WT RVFW myocytes than in WT LVFW myocytes. In Pkp2-Het hearts, similar differences were observed between RVFW and LVFW myocytes, but their amplitudes remained in the same order as WT hearts (Table 2). Altogether, these data reveal the loss of myocyte contraction is limited to the RV and not a consequence of altered excitation-contraction coupling; they suggest a direct relationship between *Pkp2* haploinsufficiency and deficient sarcomere protein function.

Altered actin regulatory pathway in the right ventricle of Pkp2-Het mice

To uncover the origins of sarcomere dysfunction in the RV of Pkp2-Het hearts, we tested whether *Pkp2* haploinsufficiency altered sarcomere gene and protein expression. Cardiac gene expression was determined by RT-qPCR using total mRNAs extracted from the LVFW and RVFW of six-month-old WT and Pkp2-Het hearts. We measured comparable expression of desmosome, sarcomere, and Ca^{2+} handling genes in ventricles from both groups (Figure 3A). Interestingly, Western blotting of RVFW homogenates from six-month-old mice revealed actin was 40% lower in Pkp2-Het hearts than in age-matched WT hearts (Figures 3B and 3C). The expression of other sarcomere proteins was similar to that of WT RVs (Figure 3C). Desmosomal and Ca^{2+} handling proteins were also unaffected by PKP2 reduction (Figures S9 and S10).

Next, to test whether the loss in actin was specific to this mouse model or a common trait of ACM hearts, we measured actin protein expression in homogenates from biopsies obtained from control and end-stage ACM explanted hearts. The Figures 3D and 3E reveal a 40% decrease in actin expression in the RV of human ACM hearts.

Phosphorylation of troponin-I and the cardiac isoform of the myosin-binding protein C (cMyBP-C), respectively, decreases Ca^{2+} sensitivity of myofilaments and increases the cooperative recruitment of cross-bridges to enhance contraction during sympathetic activation[26]. Thus, we tested whether compensatory upregulation of the β-adrenergic pathway occurred in Pkp2-Het RVs. Compared to WT hearts, RVs from six-month-old Pkp2-Het mice exhibited similar expression of β-adrenergic receptors, protein kinase A (PKA), Ca^{2+}/Calmodulin-dependent protein kinase-II (CaMKII), protein kinase C, protein kinase D, and protein phosphatase 2A. Phosphorylation of Ca^{2+} handling proteins by PKA and CaMKII, including ryanodine receptor type 2 (RyR2) at Ser2808 and Ser2814 and phospholamban at Ser16 and Thr17, was also unaltered (Figures S10 and S11). However,

the phosphorylation level of troponin I at Ser23/24 was 39% higher in Pkp2-Het RVFW homogenates, while we measured a tendency for increased phosphorylation of cMyBP-C at Ser282 (Figures 3F and 3G). In contrast, Western blotting of LVFW homogenates revealed normal expression of desmosomal, sarcomere, and Ca^{2+} handling proteins in the Pkp2-Het mouse (Figures S12 to S14) and a tendency for decrease actin in human end-stage ACM hearts (Figure 3E). The phosphorylation levels of cMyBP-C and troponin-I were normal in the LV of the Pkp2-Het mouse (Figures S13C to S13E). Nonetheless, mutant LVFWs had elevated phosphorylation of the RyR2 at the Ser2814 site (Figures S14D and S14E).

Next, to test whether reduced actin affected myofibril organization, we immunostained isolated myocytes, fixed in 4% paraformaldehyde, for the intermediate filament desmin, present in the intercalated disks and Z-disks. Desmin staining revealed despite reduced actin expression, the sarcomere lengths of Pkp2-Het LVFW and RVFW myocytes were similar to those of WT cells (Figure S15), confirming measurements we obtained in isolated myocytes paced at 0.5 Hz (Table 1). However, we observed mutant RVFW myocyte length and width tended to decrease causing an 11% reduction in cell surface area ($P<0.05$), while LVFW myocytes exhibited similar sizes to those of WT hearts (Figure S16).

To uncover the mechanisms causing a decrease in actin in Pkp2-Het RVs, we first tested whether *Pkp2* haploinsufficiency altered the desmosomes organization and caused the widening of cell-to-cell contacts[7]. We used transmission electron microscopy to examine intercalated disk ultrastructure of hearts from six-month-old Pkp2-Het mice. As shown in Figure 4A and Figure S17, *Pkp2* haploinsufficiency resulted in partial widening of cell-to-cell contacts in both ventricles, while myofibril structures were unaffected. Then, we tested whether PKP2 reduction promoted cardiomyocyte apoptosis[27] and eventually protein oxidation. We determined the percentage of TUNEL-positive nuclei in paraffin-embedded cross-sections from six-month-old hearts (Figure 4B). Figure 4C shows the number of apoptotic nuclei was increased by 2.6 times in the RVFW of Pkp2-Het hearts compared to that in WT RVs. Next, we estimated the oxidation level of cardiac proteins using the 2, 4-dinitrophenylhydrazine (2, 4-DNP) detection method. The 2, 4-DNP staining revealed the oxidation of mutant RVFW and LVFW proteins was comparable to that of age-matched WT hearts (Figure 4D and Figure S18). To further assess whether the loss of actin could be due to its oxidation[28,29], we immunoprecipitated actin from homogenates using a cardiac-specific anti-actin antibody followed by 2, 4-DNP staining. As shown in Figures 4E and 4F, actin oxidation was two times higher in the RV of Pkp2-Het hearts than that in WT RVs. In contrast, in Pkp2-Het LVs, both the number of TUNEL-positive nuclei and the oxidation of actin were comparable to those of WT LVs (Figures 4C and 4F).

Pkp2 haploinsufficiency does not promote fibrosis and fat infiltration in sedentary mice

A classic histopathology marker of the ACM phenotype is the progressive replacement of cardiac myocytes by interstitial fibrosis and fat infiltration[30]. This phenomenon particularly affects the RV in the “triangle of dysplasia”[30]. To determine whether the progressive RV dysfunction observed in sedentary aging Pkp2-Het mice was associated with fibrosis and fat infiltration, we performed classic histologic assessment (Figures 5A and 5B). Hematoxylin and eosin staining confirmed the overall normal shape of the mutant heart.

This staining also revealed normal organization of cardiac myocytes in LVs and RVs of twelve-month-old Pkp2-Het hearts (Figures 5A and 5B). Collagen staining by picrosirius red showed a tendency toward increased collagen deposits in Pkp2-Het hearts, while oil red O staining showed an absence of lipid accumulation in mutant ventricles (Figures 5B and 5C). In agreement with these data, we observed no major alterations of the Wnt/β-catenin pathway, which participates in ACM progression[31,32]. The expression of β-catenin and its phosphorylation level at Ser33/35 and Thr41, which dictate its activity (the phosphorylation causes β-catenin degradation and activation of adipogenesis, while dephosphorylation leads to β-catenin translocation to the nucleus where it activates hypertrophic transcription factors), were comparable between Pkp2-Het and WT hearts. Similarly, the expression of Glycogen Synthase Kinase 3-β (GSK3-β), the β-catenin kinase, and its phosphorylation at Ser9, active form, were also unaltered in the Pkp2-Het heart (Figures 5D and 5E).

Pkp2 haploinsufficiency increases the occurrence of life-threatening arrhythmias

The first clinical sign of ACM is often ventricular arrhythmias and aborted SCD. Previous Pkp2 animal models showed increased PR intervals and susceptibility to arrhythmias due to loss of Na^+ channel function, similar to Brugada syndrome[7]. Here, we tested whether Pkp2 haploinsufficiency alters the electrical activity of the heart and its sensitivity to ventricular arrhythmias. We recorded surface ECGs in six-month-old, anesthetized mice. In baseline conditions, Pkp2-Het mice exhibited normal heart rates as well as normal PR and QTc intervals (Figures 6A and 6B, and Table S5). Notably, Western blotting of Pkp2-Het homogenates revealed a tendency for a decrease in Na^+ channel expression in RV myocytes compared to that in LV myocytes (Figure S19). Isoproterenol (2 $mg.kg^{-1}$) supplemented with caffeine (120 $mg.kg^{-1}$) activated the β-adrenergic pathway and increased heart rates by 20% in Pkp2-Het and WT mice ($P<0.001$ vs. baseline). Nonetheless, the sympathetic activation of Pkp2-Het hearts led to higher frequencies of non-sustained (≤5 seconds) and sustained (>5 seconds) arrhythmias compared to those of WT hearts. Among these events, we recorded episodes of monomorphic and polymorphic ventricular tachycardia. Moreover, we observed that 57% of stimulated Pkp2-Het mice died prematurely from ventricular fibrillation followed by SCD (Figures 6C to 6E and Figure S19). To test whether these arrhythmias have cellular origins, we recorded Ca^{2+} transients of isolated myocytes paced (1 Hz at RT) in the presence of 100 nM isoproterenol. Both RVFW and LVFW myocytes isolated from WT and Pkp2-Het hearts responded to sympathetic stimulation by a classic increase in Ca^{2+} transient amplitudes and SR Ca^{2+} loads (Figures 6F to 6H versus Figures 2F to 2H and Figures S8 and S20). Nonetheless, we observed an enhanced inotropic response in LVFW myocytes from Pkp2-Het hearts occurring in animals as young as three months of age (Figures 6G and 6H, and Table S6).

Discussion

ACM is characterized by electrical abnormalities, cardiac remodeling, and ventricular dysfunction. Although the pathogenic variants of *PKP2* are present in most ACM clinical cases, the outcomes of these variants remain uncertain, thus preventing the development of therapeutic approaches. Here, we studied the key mechanisms of ACM progression in a novel genetically engineered mouse model expressing a known human *PKP2* pathogenic

mutation[6,10,11]. In mice, this variant causes *Pkp2* haploinsufficiency associated with altered actin expression and oxidation in RV myocytes only, causing loss of contraction and a progressive RV dysfunction. The RV-dominant ACM phenotype of the mouse is in agreement with clinical observations of ACM patients carrying *PKP2* variants[2,10].

The primary feature of this new mouse model is quasi-inhibition of mutant *Pkp2* mRNA transcripts in both ventricles of Het hearts, causing *Pkp2* haploinsufficiency. Haploinsufficiency occurs in various human disorders and animal models associated with a truncation variant, including human clinical cases of *PKP2*-mediated ACM (e.g., p.L401PfsX5 and p.L452X)[19]. Nonfunctional mRNA transcript degradation occurs during translation by nonsense-mediated mRNA decay, which identifies and promotes the denaturation of transcripts carrying an early stop codon[17]. In the Pkp2-L362fsX21 homozygous mouse, the potential absence of PKP2 protein caused early lethality during embryogenesis, demonstrating the central role played by desmosomes during development[14,16].

The progression of ACM pathology occurs in three stages: 1) the early “concealed” stage where life-threatening ventricular arrhythmias and SCD arise before ventricular remodeling; 2) the “electrical” stage where fibrosis and fat infiltrate one ventricle, usually the RV; and 3) the “late” stage where both ventricles exhibit fibro-fatty infiltration[2,30]. During their first year of life, our sedentary Pkp2-Het mice progressively developed the clinical characteristics of the early concealed stage of ACM, including high propensity for ventricular arrhythmias during stress and efforts in absence of cardiac remodeling. Similar to our mouse model, the presence of fibro-fatty infiltration is rarely reported in the hearts of sedentary *Pkp2*-mediated ACM models[7,8,23,33]. Conversely, electrical abnormalities and defects in conduction velocity (e.g., increased QRS duration) are more common and to some extent, mimic the clinical outcomes of catecholaminergic polymorphic ventricular tachycardia[34] or Brugada syndrome[35]. Thus, altered electrical activity in the heart has been linked to impaired ion channel expression and/or trafficking causing intracellular Ca^{2+} and Na^{+} mishandling[22,36,37]. Here, Pkp2-Het mice showed normal heart rates and QRS complexes, although RVFWs and LVFWs exhibited a disparity in Na^{+} channel expression. Isoproterenol and caffeine stimulated the sympathetic pathway, exacerbating the arrhythmogenic potential of the mutant heart and triggering arrhythmic events typically observed in ACM cases[38], including the patients carrying the *c.1212InsT* variant[6,10,11]. We could identify two sources of arrhythmia in Pkp2-Het LV myocytes: first, the enhanced inotropic response during isoproterenol stimulations and second, the elevated phosphorylation of RyR2 at Ser2814. The hyperphosphorylation of RyR2 increases the stochastic activity of the channel, causing Ca^{2+} leak from the SR during diastole. In the presence of elevated SR Ca^{2+} contents, RyR2-mediated Ca^{2+} leak can be large enough to 1) prematurely activate neighboring RyR2 channels (Ca^{2+} sparks) and propagate throughout the myocyte as Ca^{2+} waves; and 2) cause the depolarization of the sarcolemma via the NCX-1, triggering action potentials and ectopic beats[39]. In line with our observations, recent publications suggest increased RyR2 phosphorylation is the major source of arrhythmias in ACM hearts[9,40].

Our data demonstrate the *Pkp2*-c.*1086InsT* knock-in mutation reproduces in mice the hallmarks of human RV-dominant ACM phenotype associated with the *PKP2-c.1212InsT*

variant, including the high sensitivity to arrhythmias, ventricular tachycardia and SCD[6,10,11]. Our major contribution is identifying a progressive loss in RV contraction directly correlated with the reduction in RV cardiomyocyte function. Global loss of myocyte contraction occurred at 1 Hz, a low pacing frequency for mouse cardiomyocytes. Interestingly, intracellular Ca^{2+} transients and SR Ca^{2+} loads were normal in all tested myocytes, including those from twelve-month-old Pkp2-Het mice, suggesting reduced PKP2 directly affected sarcomere function. We confirmed this hypothesis by demonstrating 40% decreased actin in RV myocytes. This decrease left sarcomere organization unscathed compared to that in age-matched WT mice. These data are consistent with recent publications suggesting actin involvement in the development of ACM pathogenesis[41,42]. Finally, we demonstrated that loss of actin is a molecular characteristic of RVs from end-stage human ACM hearts.

Interestingly, actin oxidation took place in mutant RVs only, in parallel with elevated apoptosis and despite the fact widening of cell-to-cell contacts—a direct outcome of PKP2 reduction—occurred in both ventricles. This finding suggests the *PKP2*-mediated ACM phenotype develops from the physiological properties of the RV rather than genetic regulations. Indeed, LV and RV myocytes share similar excitation-contraction coupling properties, yet structural differences in RV versus LV (e.g., thickness, shape…) lead individual RV cardiomyocytes, particularly at cell-to-cell contacts, to endure higher stress and stretch conditions than do LV cardiomyocytes. Prior's group showed the RV is subjected to a 125% increase in end-systolic wall stress during exercise, while wall stress increases only by 14% in the LV[43]. In line with this, clinical evidence and ACM animal models have highlighted the effects of workload on the onset of ACM[31,44–46], thus revealing that the level of physiological stress sensed by cardiomyocytes is a major criterion for the development of the pathology. In normal housing conditions, mouse cardiac stress is limited but sufficient to impact actin stability during aging. Indeed, we report actin oxidation is doubled in the RV of six-month-old Pkp2-Het hearts compared to that in age-matched WT RVs, while the overall oxidation of cardiac proteins is unaffected. This suggests the targeted oxidation of actin is an outcome of cardiomyocyte physiological stressors that leads to a reduction in total actin and impairment of RV myocytes contraction capacity. Notably, a similar reduction in actin is observed in hearts during ischemia/reperfusion[28,29].

Our observations are consistent with recent publications showing partial and complete knock-out of *Pkp2* expression leads to slow ACM progression, widening of intercalated disks, absence of fibrosis and fat infiltration, but a high sensitivity to arrhythmias due to altered Ca^{2+} homeostasis and Na^{+} channel dysregulation. However, our findings also disagree with some of the literature, particularly with the role played by intracellular Ca^{2+} mishandling for the development of the disorder. In our case, the ACM phenotype progresses principally due to mechanical dysfunction rather than modifications of the expression profile of Ca^{2+} handling protein genes[9,22,23]. The reasons for the differences in our data remain unclear, but we hypothesize they could be due to the nature of the animal model tested: a knock-in mouse model reproducing a human variant in this study versus knock-out models in other studies[9,22,23].

In conclusion, our data demonstrate that the *Pkp2-c.1086InsT* variant associates with progressive development of the hallmarks of the ACM early "concealed" stage and reveal

actin's role in disease development, particularly its implication in the RV. In classic human ACM cases, the workload of the heart largely contributes to disease onset. Thus, actin as a marker of disease progression represents a novel approach for early detection and future therapeutics. However, some questions remain regarding the effect of increased workload on Pkp2-Het myocyte contraction and the possible role of actin in the development of later stages of ACM.

Supplementary Material

Refer to Web version on PubMed Central for supplementary material.

Acknowledgments

The authors acknowledge the excellent advice and recommendations from Dr. Salvatore Mancarella and Dr. Glenn Wetzel during the research study. We also thank Dr. Courtney Bricker-Anthony for careful editing of the manuscript.

Sources of Funding

This work was supported by the NIH-National Heart Lung and Blood Institute grant HL-116906 (JAT), the 2016 and 2017 Junior Faculty Grant from the Le Bonheur Children's Hospital Foundation (EMC), and the 2016 Bea Gerber Award (EMC).

Non-Standard Abbreviations and Acronyms:

2, 4-DNP	2, 4-dinitrophenylhydrazine
ACM	Arrhythmogenic cardiomyopathy
β-Cat	β-Catenin
CaMKII	Ca2+/Calmodulin-dependent kinase II
CSQ2	Calsequestrin 2
GSK3-β	Glycogen Synthase Kinase 3-β
LVFW and RVFW	Left and right ventricular free wall
cMyBP-C	Myosin-binding protein C, Cardiac isoform
α-MHC	Myosin heavy chain type α
NCX-1	Na+/Ca2+ exchanger type 1
PKA	Protein kinase A
PKP2	Plakophilin-2
RyR2	Ryanodine receptor type 2
SCD	Sudden cardiac death
TAPSE	Tricuspid annular plane systolic excursion

Tn-I	Troponin-I
TPM	Tropomyosin

References

1. Awad MM, Calkins H, Judge DP. Mechanisms of disease: molecular genetics of arrhythmogenic right ventricular dysplasia/cardiomyopathy. Nat Clin Pract Cardiovasc Med. 2008;5:258–267. doi: 10.1038/ncpcardio1182 [PubMed: 18382419]
2. Towbin JA. Inherited cardiomyopathies. Circulation journal : official journal of the Japanese Circulation Society. 2014;78:2347–2356. doi: 10.1253/circj.cj-14-0893 [PubMed: 25186923]
3. Saguner AM, Brunckhorst C, Duru F. Arrhythmogenic ventricular cardiomyopathy: A paradigm shift from right to biventricular disease. World journal of cardiology. 2014;6:154–174. doi: 10.4330/wjc.v6.i4.154 [PubMed: 24772256]
4. Corrado D, Basso C, Judge DP. Arrhythmogenic Cardiomyopathy. Circulation research. 2017;121:784–802. doi: 10.1161/CIRCRESAHA.117.309345 [PubMed: 28912183]
5. Nekrasova O, Green KJ. Desmosome assembly and dynamics. Trends in cell biology. 2013;23:537–546. doi: 10.1016/j.tcb.2013.06.004 [PubMed: 23891292]
6. van Tintelen JP, Entius MM, Bhuiyan ZA, Jongbloed R, Wiesfeld AC, Wilde AA, van der Smagt J, Boven LG, Mannens MM, van Langen IM, et al. Plakophilin-2 mutations are the major determinant of familial arrhythmogenic right ventricular dysplasia/cardiomyopathy. Circulation. 2006;113:1650–1658. doi: 10.1161/CIRCULATIONAHA.105.609719 [PubMed: 16567567]
7. Cerrone M, Lin X, Zhang M, Agullo-Pascual E, Pfenniger A, Chkourko Gusky H, Novelli V, Kim C, Tirasawadichai T, Judge DP, et al. Missense mutations in plakophilin-2 cause sodium current deficit and associate with a Brugada syndrome phenotype. Circulation. 2014;129:1092–1103. doi: 10.1161/CIRCULATIONAHA.113.003077 [PubMed: 24352520]
8. Moncayo-Arlandi J, Guasch E, Sanz-de la Garza M, Casado M, Garcia NA, Mont L, Sitges M, Knoll R, Buyandelger B, Campuzano O, et al. Molecular disturbance underlies to arrhythmogenic cardiomyopathy induced by transgene content, age and exercise in a truncated PKP2 mouse model. Hum Mol Genet. 2016;25:3676–3688. doi: 10.1093/hmg/ddw213 [PubMed: 27412010]
9. Kim JC, Perez-Hernandez Duran M, Alvarado FJ, Maurya SR, Montnach J, Yin Y, Zhang M, Lin X, Vasquez C, Heguy A, et al. Disruption of Ca(2+)i Homeostasis and Cx43 Hemichannel Function in the Right Ventricle Precedes Overt Arrhythmogenic Cardiomyopathy in PKP2-Deficient Mice. Circulation. 2019. doi: 10.1161/CIRCULATIONAHA.119.039710
10. Xu T, Yang Z, Vatta M, Rampazzo A, Beffagna G, Pilichou K, Pillichou K, Scherer SE, Saffitz J, Kravitz J, et al. Compound and digenic heterozygosity contributes to arrhythmogenic right ventricular cardiomyopathy. Journal of the American College of Cardiology. 2010;55:587–597. doi: 10.1016/j.jacc.2009.11.020 [PubMed: 20152563]
11. Noorman M, Hakim S, Kessler E, Groeneweg JA, Cox MG, Asimaki A, van Rijen HV, van Stuijvenberg L, Chkourko H, van der Heyden MA, et al. Remodeling of the cardiac sodium channel, connexin43, and plakoglobin at the intercalated disk in patients with arrhythmogenic cardiomyopathy. Heart Rhythm. 2013;10:412–419. doi: 10.1016/j.hrthm.2012.11.018 [PubMed: 23178689]
12. Huby A-C, Mendsaikhan U, Takagi K, Martherus R, Wansapura J, Gong N, Osinska H, James JF, Kramer K, Saito K, et al. Disturbance in Z-disk mechanosensitive proteins induced by a persistent mutant myopalladin causes familial restrictive cardiomyopathy. Journal of the American College of Cardiology. 2014;64:2765–2776. doi: 10.1016/j.jacc.2014.09.071 [PubMed: 25541130]
13. Cerrone M, Colombi B, Santoro M, di Barletta MR, Scelsi M, Villani L, Napolitano C, Priori SG. Bidirectional ventricular tachycardia and fibrillation elicited in a knock-in mouse model carrier of a mutation in the cardiac ryanodine receptor. Circ Res. 2005;96:e77–82. doi: 10.1161/01.RES.0000169067.51055.72 [PubMed: 15890976]
14. Bierkamp C, McLaughlin KJ, Schwarz H, Huber O, Kemler R. Embryonic heart and skin defects in mice lacking plakoglobin. Dev Biol. 1996;180:780–785. doi: 10.1006/dbio.1996.0346 [PubMed: 8954745]

15. Gallicano GI, Kouklis P, Bauer C, Yin M, Vasioukhin V, Degenstein L, Fuchs E. Desmoplakin is required early in development for assembly of desmosomes and cytoskeletal linkage. The Journal of cell biology. 1998;143:2009–2022. doi: 10.1083/jcb.143.7.2009 [PubMed: 9864371]

16. Grossmann KS, Grund C, Huelsken J, Behrend M, Erdmann B, Franke WW, Birchmeier W. Requirement of plakophilin 2 for heart morphogenesis and cardiac junction formation. The Journal of cell biology. 2004;167:149–160. doi: 10.1083/jcb.200402096 [PubMed: 15479741]

17. Miller JN, Pearce DA. Nonsense-mediated decay in genetic disease: friend or foe? Mutation research Reviews in mutation research. 2014;762:52–64. doi: 10.1016/j.mrrev.2014.05.001 [PubMed: 25485595]

18. Kim C, Wong J, Wen J, Wang S, Wang C, Spiering S, Kan NG, Forcales S, Puri PL, Leone TC, et al. Studying arrhythmogenic right ventricular dysplasia with patient-specific iPSCs. Nature. 2013;494:105–110. doi: 10.1038/nature11799 [PubMed: 23354045]

19. Rasmussen TB, Nissen PH, Palmfeldt J, Gehmlich K, Dalager S, Jensen UB, Kim WY, Heickendorff L, Molgaard H, Jensen HK, et al. Truncating plakophilin-2 mutations in arrhythmogenic cardiomyopathy are associated with protein haploinsufficiency in both myocardium and epidermis. Circ Cardiovasc Genet. 2014;7:230–240. doi: 10.1161/CIRCGENETICS.113.000338 [PubMed: 24704780]

20. Dalal D, Molin LH, Piccini J, Tichnell C, James C, Bomma C, Prakasa K, Towbin JA, Marcus FI, Spevak PJ, et al. Clinical features of arrhythmogenic right ventricular dysplasia/cardiomyopathy associated with mutations in plakophilin-2. Circulation. 2006;113:1641–1649. doi: 10.1161/CIRCULATIONAHA.105.568642 [PubMed: 16549640]

21. Alcalde M, Campuzano O, Berne P, Garcia-Pavia P, Doltra A, Arbelo E, Sarquella-Brugada G, Iglesias A, Alonso-Pulpon L, Brugada J, et al. Stop-gain mutations in PKP2 are associated with a later age of onset of arrhythmogenic right ventricular cardiomyopathy. PLoS One. 2014;9:e100560. doi: 10.1371/journal.pone.0100560

22. Cerrone M, Montnach J, Lin X, Zhao YT, Zhang M, Agullo-Pascual E, Leo-Macias A, Alvarado FJ, Dolgalev I, Karathanos TV, et al. Plakophilin-2 is required for transcription of genes that control calcium cycling and cardiac rhythm. Nat Commun. 2017;8:106. doi: 10.1038/s41467-017-00127-0 [PubMed: 28740174]

23. van Opbergen CJM, Noorman M, Pfenniger A, Copier JS, Vermij SH, Li Z, van der Nagel R, Zhang M, de Bakker JMT, Glass AM, et al. Plakophilin-2 Haploinsufficiency Causes Calcium Handling Deficits and Modulates the Cardiac Response Towards Stress. Int J Mol Sci. 2019;20. doi: 10.3390/ijms20174076

24. Camors E, Mohler PJ, Bers DM, Despa S. Ankyrin-B reduction enhances Ca spark-mediated SR Ca release promoting cardiac myocyte arrhythmic activity. Journal of molecular and cellular cardiology. 2012;52:1240–1248. doi: 10.1016/j.yjmcc.2012.02.010 [PubMed: 22406428]

25. Bers DM. Cardiac excitation-contraction coupling. Nature. 2002;415:198–205. doi: 10.1038/415198a [PubMed: 11805843]

26. van der Velden J, Stienen GJM. Cardiac Disorders and Pathophysiology of Sarcomeric Proteins. Physiol Rev. 2019;99:381–426. doi: 10.1152/physrev.00040.2017 [PubMed: 30379622]

27. Mallat Z, Tedgui A, Fontaliran F, Frank R, Durigon M, Fontaine G. Evidence of apoptosis in arrhythmogenic right ventricular dysplasia. N Engl J Med. 1996;335:1190–1196. doi: 10.1056/NEJM199610173351604 [PubMed: 8815941]

28. Powell SR, Gurzenda EM, Wahezi SE. Actin is oxidized during myocardial ischemia. Free Radic Biol Med. 2001;30:1171–1176. doi: 10.1016/s0891-5849(01)00514-7 [PubMed: 11369508]

29. Divald A, Powell SR. Proteasome mediates removal of proteins oxidized during myocardial ischemia. Free Radic Biol Med. 2006;40:156–164. doi: 10.1016/j.freeradbiomed.2005.09.022 [PubMed: 16337889]

30. Austin KM, Trembley MA, Chandler SF, Sanders SP, Saffitz JE, Abrams DJ, Pu WT. Molecular mechanisms of arrhythmogenic cardiomyopathy. Nat Rev Cardiol. 2019;16:519–537. doi: 10.1038/s41569-019-0200-7 [PubMed: 31028357]

31. Martherus R, Jain R, Takagi K, Mendsaikhan U, Turdi S, Osinska H, James JF, Kramer K, Purevjav E, Towbin JA. Accelerated cardiac remodeling in desmoplakin transgenic mice in response to endurance exercise is associated with perturbed Wnt/beta-catenin signaling.

American journal of physiology Heart and circulatory physiology. 2016;310:H174–187. doi: 10.1152/ajpheart.00295.2015 [PubMed: 26545710]

32. Camors EM, Purevjav E, Jefferies JL, Saffitz JE, Gong N, Ryan TD, Lucky AW, Taylor MD, Sullivan LM, Mestroni L, et al. Early Lethality Due to a Novel Desmoplakin Variant Causing Infantile Epidermolysis Bullosa Simplex with Fragile Skin, Aplasia Cutis Congenita, and Arrhythmogenic Cardiomyopathy. Circ Genom Precis Med. 2020. doi: 10.1161/CIRCGEN.119.002800
33. Gomes J, Finlay M, Ahmed AK, Ciaccio EJ, Asimaki A, Saffitz JE, Quarta G, Nobles M, Syrris P, Chaubey S, et al. Electrophysiological abnormalities precede overt structural changes in arrhythmogenic right ventricular cardiomyopathy due to mutations in desmoplakin-A combined murine and human study. Eur Heart J. 2012;33:1942–1953. doi: 10.1093/eurheartj/ehr472 [PubMed: 22240500]
34. Tester DJ, Ackerman JP, Giudicessi JR, Ackerman NC, Cerrone M, Delmar M, Ackerman MJ. Plakophilin-2 Truncation Variants in Patients Clinically Diagnosed With Catecholaminergic Polymorphic Ventricular Tachycardia and Decedents With Exercise-Associated Autopsy Negative Sudden Unexplained Death in the Young. JACC Clin Electrophysiol. 2019;5:120–127. doi: 10.1016/j.jacep.2018.09.010 [PubMed: 30678776]
35. Corrado D, Zorzi A, Cerrone M, Rigato I, Mongillo M, Bauce B, Delmar M. Relationship Between Arrhythmogenic Right Ventricular Cardiomyopathy and Brugada Syndrome: New Insights From Molecular Biology and Clinical Implications. Circulation Arrhythmia and electrophysiology. 2016;9:e003631. doi: 10.1161/CIRCEP.115.003631
36. Sato PY, Musa H, Coombs W, Guerrero-Serna G, Patino GA, Taffet SM, Isom LL, Delmar M. Loss of plakophilin-2 expression leads to decreased sodium current and slower conduction velocity in cultured cardiac myocytes. Circ Res. 2009;105:523–526. doi: 10.1161/CIRCRESAHA.109.201418 [PubMed: 19661460]
37. Cerrone M, Noorman M, Lin X, Chkourko H, Liang FX, van der Nagel R, Hund T, Birchmeier W, Mohler P, van Veen TA, et al. Sodium current deficit and arrhythmogenesis in a murine model of plakophilin-2 haploinsufficiency. Cardiovasc Res. 2012;95:460–468. doi: 10.1093/cvr/cvs218 [PubMed: 22764151]
38. Basso C, Corrado D, Marcus FI, Nava A, Thiene G. Arrhythmogenic right ventricular cardiomyopathy. Lancet. 2009;373:1289–1300. doi: 10.1016/S0140-6736(09)60256-7 [PubMed: 19362677]
39. Camors E, Valdivia HH. CaMKII regulation of cardiac ryanodine receptors and inositol triphosphate receptors. Frontiers in pharmacology. 2014;5:101. doi: 10.3389/fphar.2014.00101 [PubMed: 24847270]
40. Wang Y, Li C, Shi L, Chen X, Cui C, Huang J, Chen B, Hall DD, Pan Z, Lu M, et al. Integrin beta1D Deficiency-Mediated RyR2 Dysfunction Contributes to Catecholamine-Sensitive Ventricular Tachycardia in Arrhythmogenic Right Ventricular Cardiomyopathy. Circulation. 2020;141:1477–1493. doi: 10.1161/CIRCULATIONAHA.119.043504 [PubMed: 32122157]
41. Kant S, Freytag B, Herzog A, Reich A, Merkel R, Hoffmann B, Krusche CA, Leube RE. Desmoglein 2 mutation provokes skeletal muscle actin expression and accumulation at intercalated discs in murine hearts. J Cell Sci. 2019;132. doi: 10.1242/jcs.199612
42. Puzzi L, Borin D, Gurha P, Lombardi R, Martinelli V, Weiss M, Andolfi L, Lazzarino M, Mestroni L, Marian AJ, et al. Knock Down of Plakophillin 2 Dysregulates Adhesion Pathway through Upregulation of miR200b and Alters the Mechanical Properties in Cardiac Cells. Cells. 2019;8. doi: 10.3390/cells8121639
43. La Gerche A, Heidbuchel H, Burns AT, Mooney DJ, Taylor AJ, Pfluger HB, Inder WJ, Macisaac AI, Prior DL. Disproportionate exercise load and remodeling of the athlete's right ventricle. Med Sci Sports Exerc. 2011;43:974–981. doi: 10.1249/MSS.0b013e31820607a3 [PubMed: 21085033]
44. James CA, Bhonsale A, Tichnell C, Murray B, Russell SD, Tandri H, Tedford RJ, Judge DP, Calkins H. Exercise increases age-related penetrance and arrhythmic risk in arrhythmogenic right ventricular dysplasia/cardiomyopathy-associated desmosomal mutation carriers. J Am Coll Cardiol. 2013;62:1290–1297. doi: 10.1016/j.jacc.2013.06.033 [PubMed: 23871885]
45. Te Riele A, James CA, Sawant AC, Bhonsale A, Groeneweg JA, Mast TP, Murray B, Tichnell C, Dooijes D, van Tintelen JP, et al. Arrhythmogenic Right Ventricular Dysplasia/Cardiomyopathy

in the Pediatric Population: Clinical Characterization and Comparison With Adult-Onset Disease. JACC Clin Electrophysiol. 2015;1:551–560. doi: 10.1016/j.jacep.2015.08.004 [PubMed: 29759408]

46. Cruz FM, Sanz-Rosa D, Roche-Molina M, Garcia-Prieto J, Garcia-Ruiz JM, Pizarro G, Jimenez-Borreguero LJ, Torres M, Bernad A, Ruiz-Cabello J, et al. Exercise triggers ARVC phenotype in mice expressing a disease-causing mutated version of human plakophilin-2. J Am Coll Cardiol. 2015;65:1438–1450. doi: 10.1016/j.jacc.2015.01.045 [PubMed: 25857910]

Clinical Perspective

What is new?

- In a novel knock-in mouse model of Plakophilin-2-mediated arrhythmogenic cardiomyopathy, aging associates with right ventricular dysfunction due to reduced myocyte contractions.
- Actin reduction is a characteristic of the right ventricle from both mutant mouse hearts (−40% versus age-matched WT hearts) and biopsies from end-stage arrhythmogenic cardiomyopathy patients (−40% versus control hearts).
- Adrenergic stimulation of plakophilin-2 mutant mice reveals Ca^{2+} overload in left ventricular myocytes and high propensity of the hearts to life-threatening ventricular arrhythmias (57% of mutant mice died from sudden cardiac death).

What are the clinical implications?

- Early development of arrhythmogenic cardiomyopathy is due to the mechanical and physiological stress of the right ventricle.
- Actin is revealed as a major contributor to early-stage arrhythmogenic cardiomyopathy, and its expression is a novel marker of the disease progression.

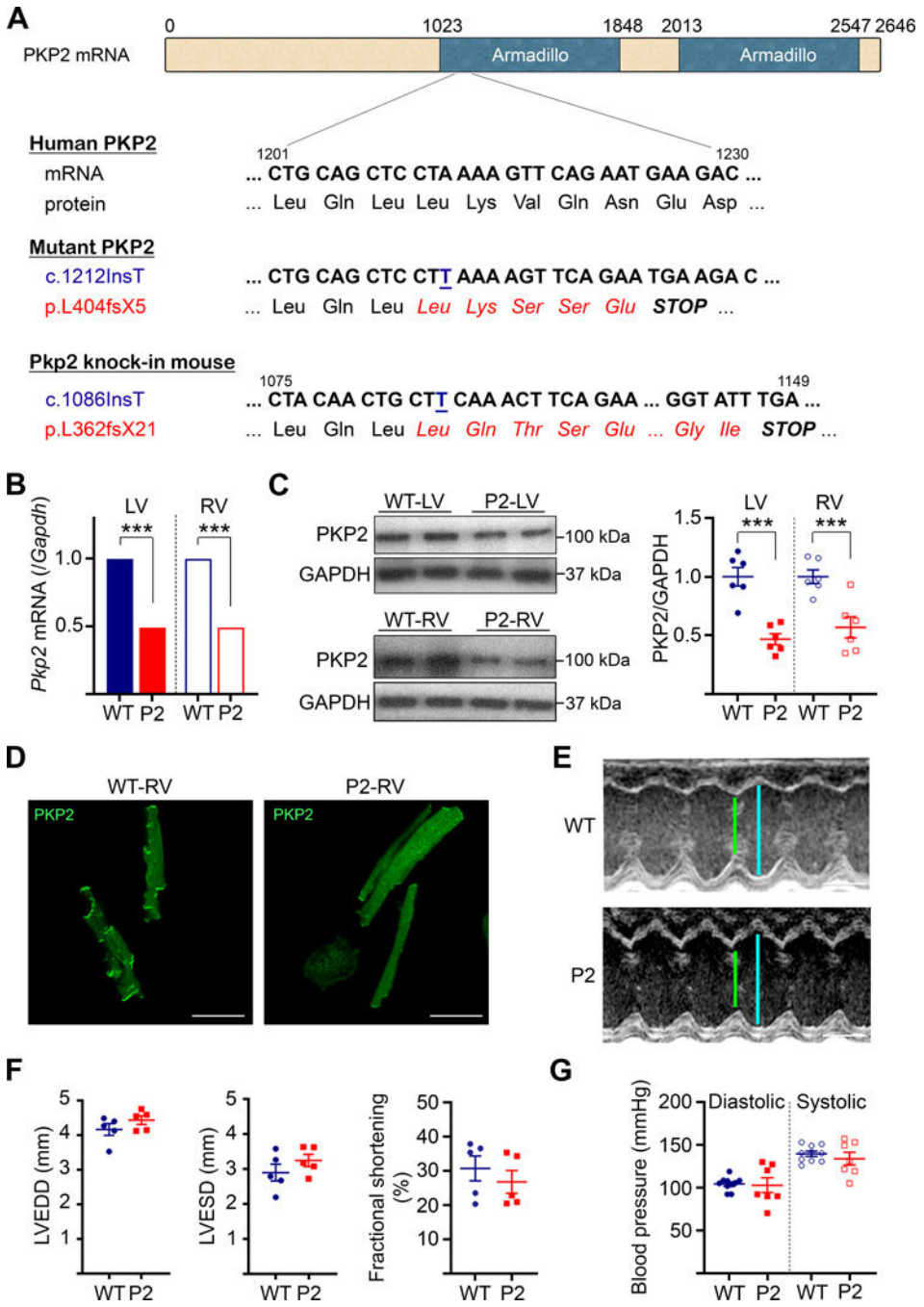

Figure 1: General characteristics of the Pkp2-Het knock-in mouse model.

A] Genetics of the Pkp2 knock-in mouse model. B and C] Quantifications of PKP2 mRNAs (RT-qPCR, ΔΔCt method with *Gapdh* as the housekeeping gene) and proteins (Western blot) reveal 50% decreased expression in Pkp2-Het hearts. N= 6 hearts per group. D] Immunohistochemistry shows PKP2 in the intercalated disks of isolated RVFW Pkp2-Het myocytes. Bar = 50 μm. E] Representative images of M-mode echocardiography of LV function in six-month-old WT and Pkp2-Het mice (green: systole, blue: diastole). Bar = 100 msec. F] Quantification of left ventricular end diastolic (LVEDD) and systolic (LVESD)

dimensions, and fractional shortening of hearts from six-month-old WT and Pkp2-Het mice. N= 5 mice per group. G] Tail blood pressure measured in conscious six-month-old WT and Pkp2-Het mice. N= 7–10 mice per group. ***: $P<0.001$ vs. WT.

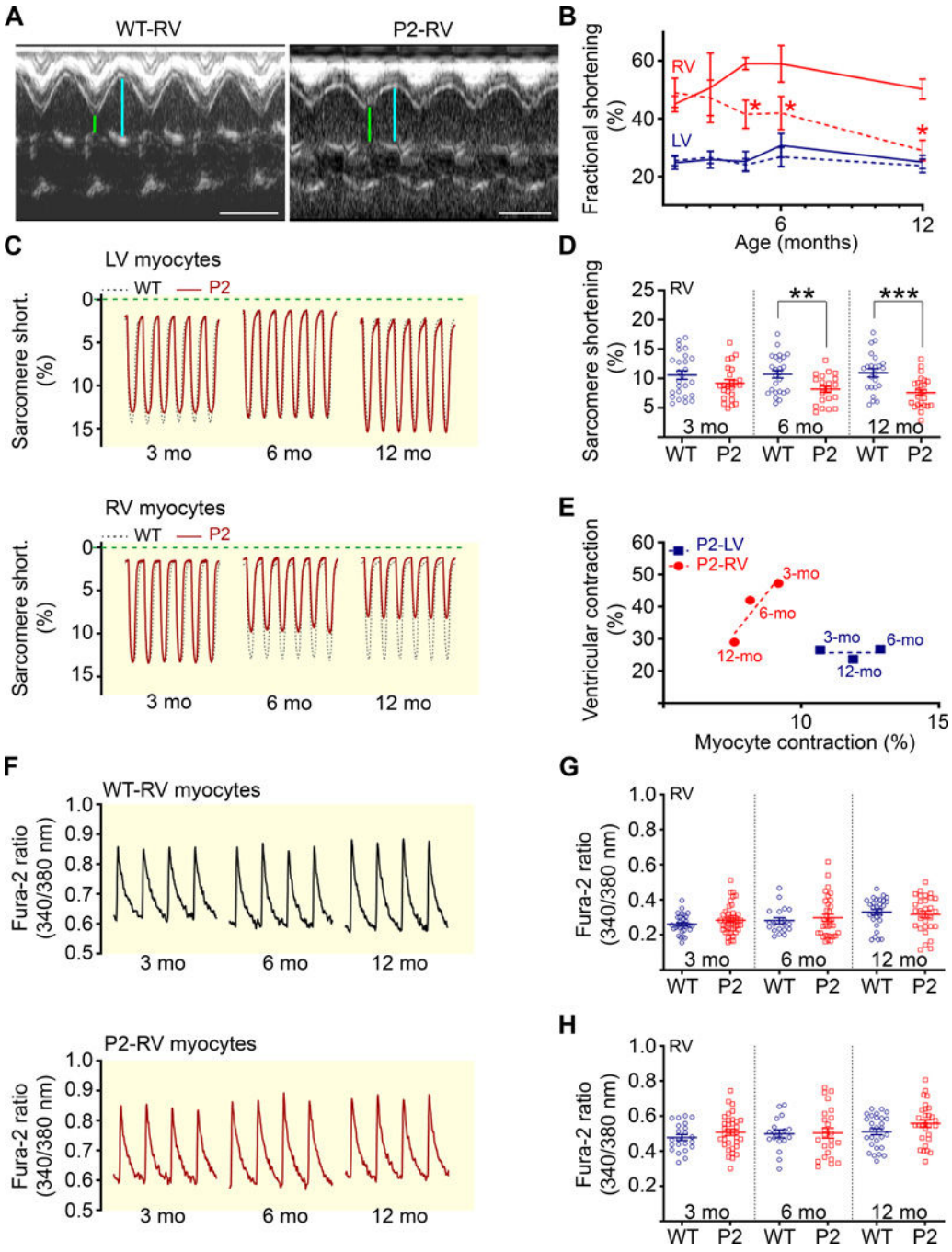

Figure 2: Pathophysiological characteristics of RV dysfunction in the Pkp2-Het knock-in mouse model.

A] Representative images of M-mode echocardiography of RV function in six-month-old WT and Pkp2-Het mice. Note the reduction in contraction during systole (green) of the mutant RV (diastole: blue). Bar = 100 msec. B] Fractional shortening in aging WT (solid lines) and Pkp2-Het (dotted lines) mice. Note that RV function continuously declined in Pkp2-Het mice older than three months. N= 5–7 mice per group. C] Impact of aging on contraction of isolated myocytes paced at 3 Hz. Top: LVFW myocytes, Bottom: RVFW myocytes. Notice the progressive reduction in sarcomere shortening in RV myocytes from

aging Pkp2-Het mice. The green dotted line (0) represents diastolic sarcomere length at 0.5 Hz. D] Age-dependent reduction in sarcomere shortening in isolated Pkp2-Het RVFW myocytes paced at 3 Hz. n= 20–26 cells per 5–6 hearts per group. E] Pkp2-Het ventricular contraction (fractional shortening) as a function of isolated myocyte sarcomere shortening. Note the correlation between the age-dependent loss of RV function and the reduction in RVFW myocyte contraction. By contrast, the LV is unaffected. F] Representative recordings of Ca^{2+} transients in RVFW myocytes from three-, six-, and twelve-month-old mice paced at 1 Hz. Representative recordings of caffeine responses are presented in Figure S8. G] Ca^{2+} transient amplitudes and H] Sarcoplasmic reticulum Ca^{2+} contents were similar in RVFW myocytes isolated from aging WT and Pkp2-Het hearts. n= 19–39 cells per 5–6 hearts per group. *: $P<0.05$, **: $P<0.01$, and ***: $P<0.001$ vs. age-matched WT.

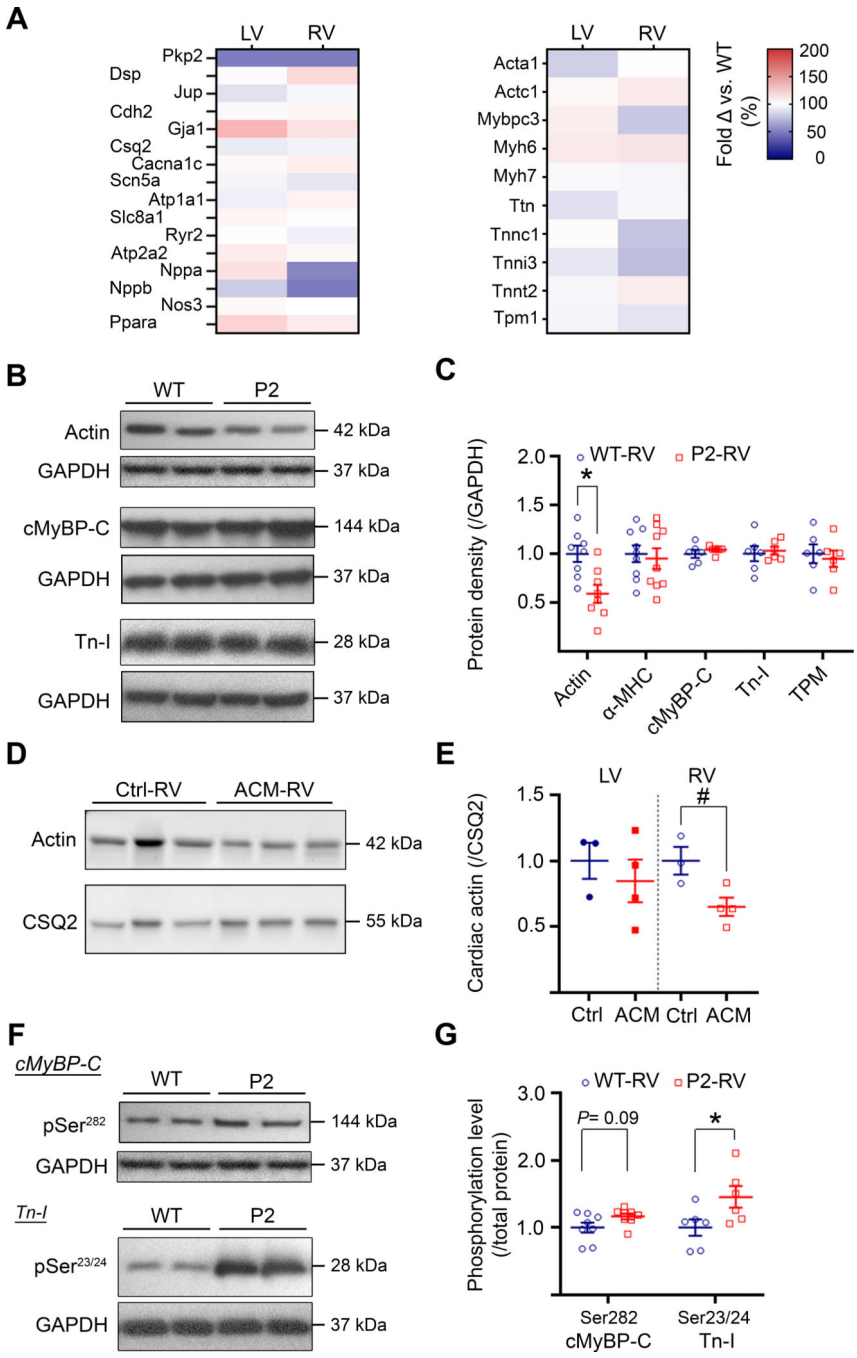

Figure 3: Effect of *Pkp2* haploinsufficiency on cardiac gene and protein expression profiles.

A] RT-qPCR data of sarcomere, Ca^{2+} handling, and intercalated disk genes. Data presented as percent of change using the ΔΔCt method with *Gapdh* as the housekeeping gene. Notably, none of the genes tested in the Pkp2-Het heart exhibit altered expression compared to those in the WT heart, except *Pkp2* and *Nppb*. N= 6 hearts per group. B] Representative Western blots of actin, cardiac myosin-binding protein C (cMyBP-C), and troponin-I (Tn-I) in RVFW homogenates from six-month-old WT and Pkp2-Het hearts. Representative Western blots of myosin heavy chain type α (α-MHC) and tropomyosin (TPM) are presented in Figure S9A.

C] Quantification of sarcomere protein expression after normalization to GAPDH. Note the 40% decrease in actin in Pkp2-Het RVs. N= 6–9 hearts per group. D] Representative Western blots of actin and calsequestrin-2 (CSQ2) in homogenates from RV biopsies of human control (Ctrl) and end-stage ACM hearts. E] Quantification of cardiac actin expression in human biopsies normalized to CSQ2. Note the 40% reduction in actin in the RV of end-stage ACM hearts. N= 3 control and 4 ACM hearts. F] Representative Western blots of cMyBP-C and Tn-I phosphorylation at Ser282 and Ser23/24, respectively, in RVFW homogenates from six-month-old WT and Pkp2-Het hearts. G] Quantification of cMyBP-C and Tn-I phosphorylation reveals 39% increased phosphorylation of Tn-I in the RV of Pkp2-Het hearts. N= 6–9 hearts per group. *: $P<0.05$ vs. WT. #: $P<0.05$ vs. Control.

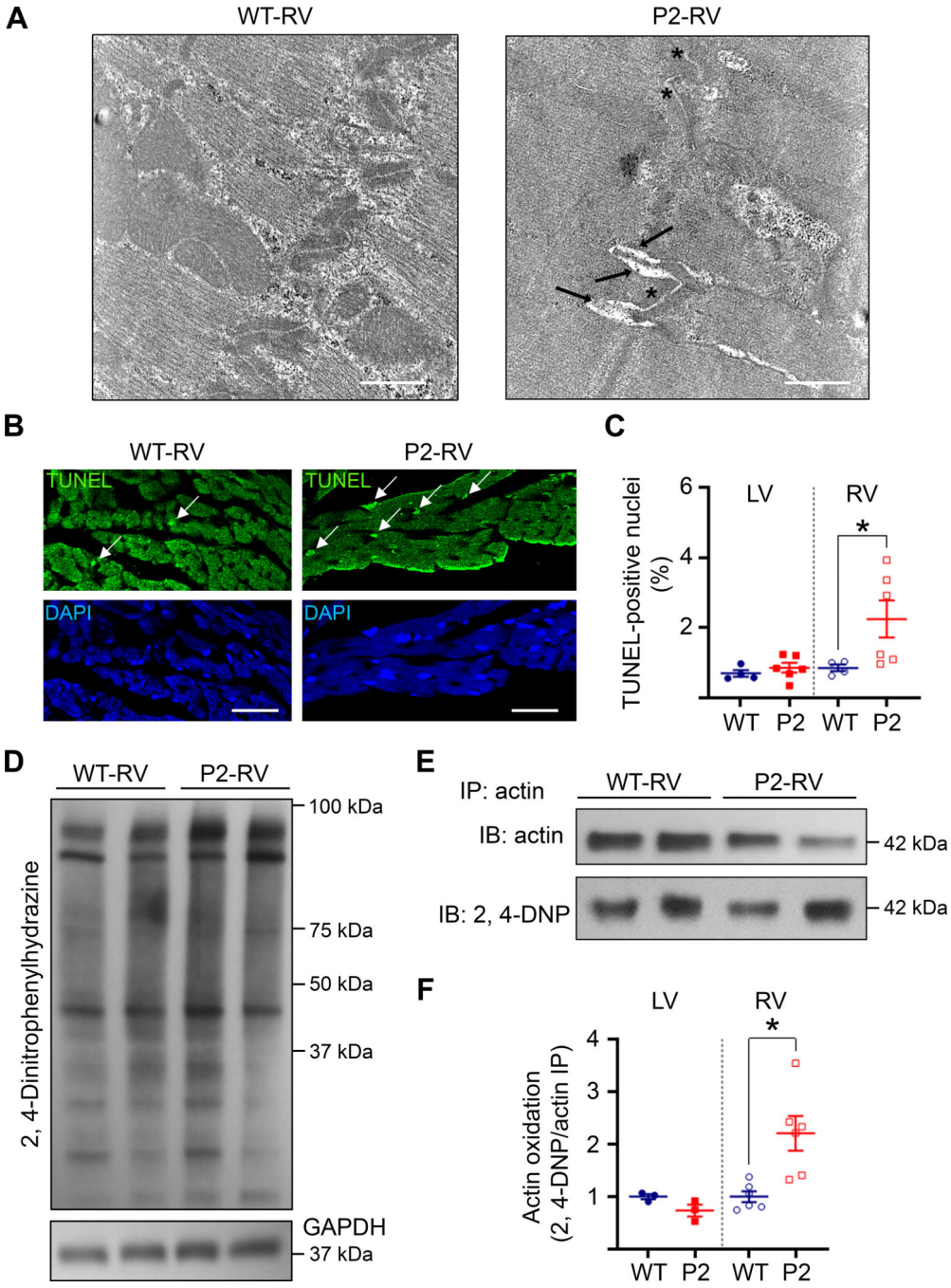

Figure 4: Outcomes of actin reduction on RV cardiomyocyte organization and protein oxidation profiles.

A] Representative images of transmission electron microscopy of RVFWs from six-month-old WT and Pkp2-Het mice. Note the concomitant presence, in intercalated disks of the mutant RV, of normal (asterisks) and widened (arrows) areas. Bar = 500 nm. B] Representative images of TUNEL-stained cardiomyocyte nuclei from six-month-old WT and Pkp2-Het RVFWs. Bar = 20 μm. C] TUNEL-positive nuclei frequency in six-month-old WT and Pkp2-Het hearts. Note the significant increase in apoptosis in the RV of Pkp2-Het hearts. n= 2,400–3,300 DAPI-stained nuclei per ventricle per heart, N= 4–6

hearts per group. D] Representative Western blot of 2, 4-DNP-stained proteins in RVFW homogenates from six-month-old WT and Pkp2-Het mice. Statistical data are presented in Figure S18. E] Representative Western blots of actin immunoprecipitation (top) and actin immunoprecipitation followed by 2, 4-DNP staining (bottom). F] Quantification of actin oxidation in homogenates from six-month-old WT and Pkp2-Het hearts. Notice the increase in actin oxidation in the RV of Pkp2-Het hearts. N= 3–6 ventricles per group. *: $P<0.05$ vs. WT.

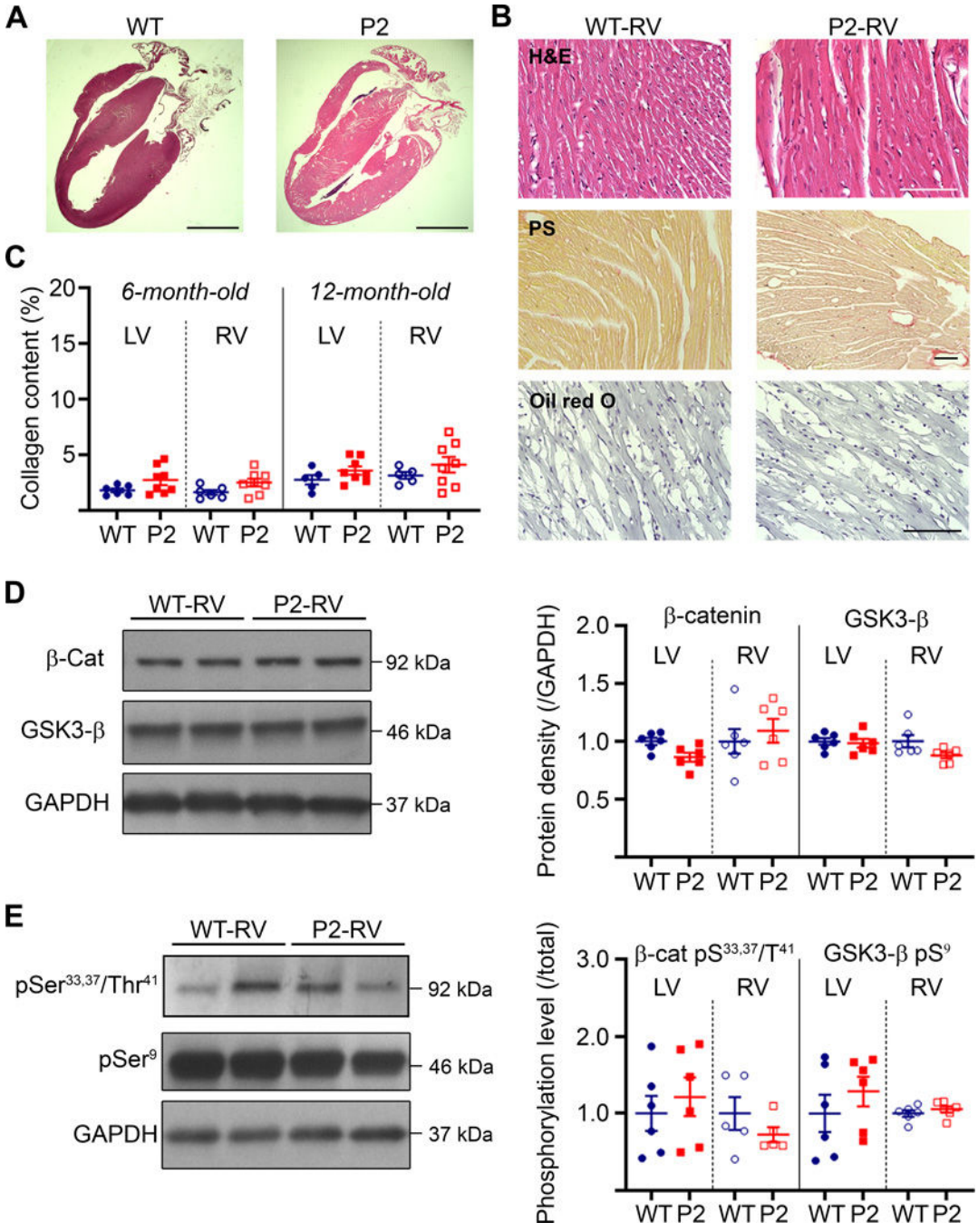

Figure 5: Histologic assessment of Pkp2-Het hearts.

A] Hematoxylin and eosin (H&E) staining reveals the absence of remodeling in the heart of twelve-month-old Pkp2-Het mice. Bar= 8 mm. B] High magnification view of H&E, picrosirius red (PS), and oil red O staining of twelve-month-old WT and Pkp2-Het hearts (Bar= 100 μm). C] Quantification of picrosirius red staining in six- and twelve-month-old hearts reveals a tendency toward increased collagen deposition in Pkp2-Het hearts. N= 5–8 hearts per group. D] β-catenin and GSK3-β expression in six-month-old WT and Pkp2-Het hearts. Left: Representative Western blots of RVFW homogenates; Right: Protein

expression normalized to GAPDH. N= 6 hearts per group. E] β-catenin and GSK3-β phosphorylation in six-month-old WT and Pkp2-Het hearts. Left: Representative Western blots of β-catenin and GSK3-β phosphorylation at Ser33,37/Thr41 and Ser9, respectively, in RVFW homogenates; Right: β-catenin (β-Cat) and GSK3-β phosphorylation normalized to total protein expression. N= 5–6 hearts per group.

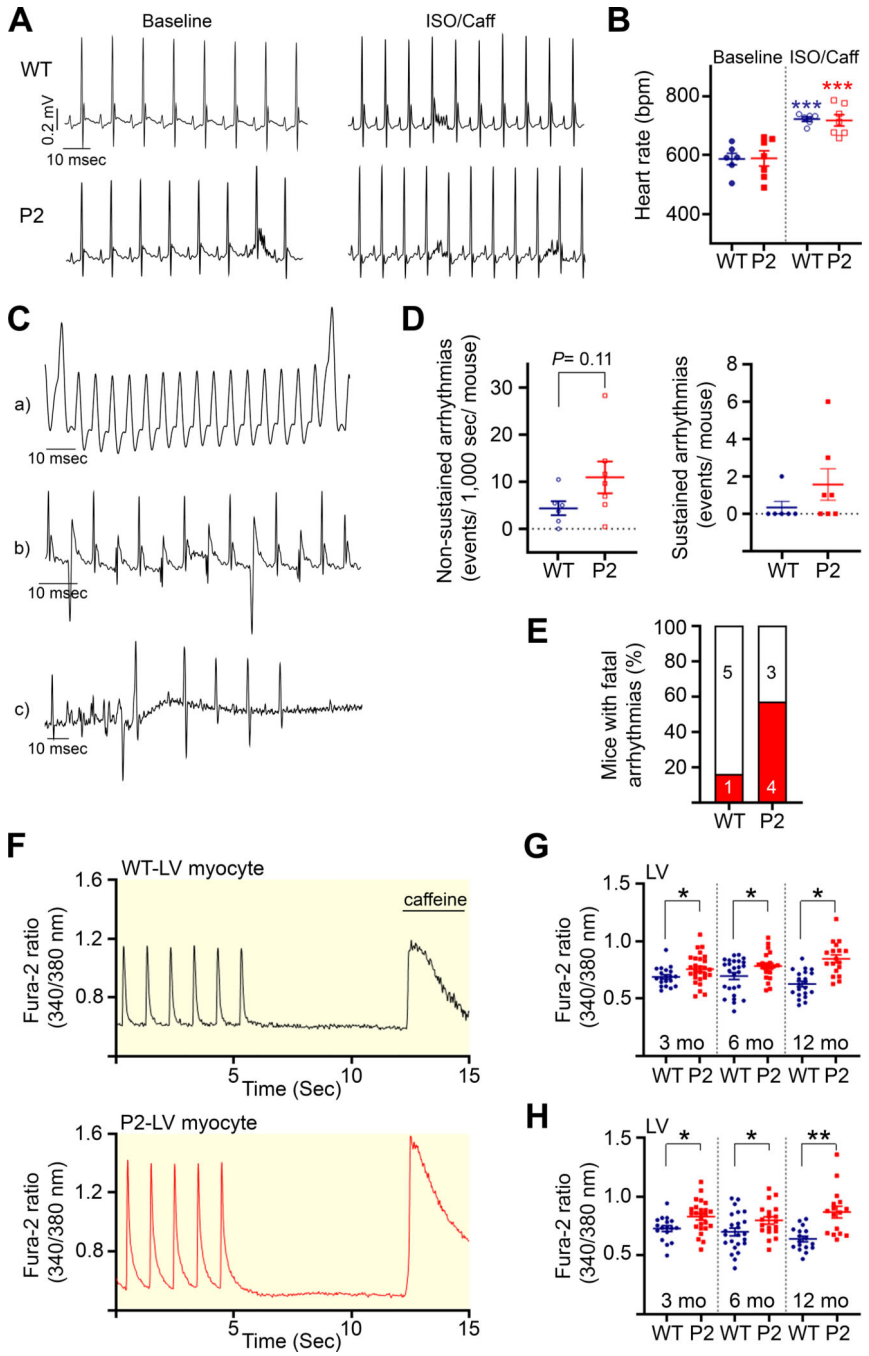

Figure 6: Effect of Pkp2 haploinsufficiency on the susceptibility of the heart to life-threatening arrhythmias.

A] Representative surface ECG recordings of six-month-old WT and Pkp2-Het mice at baseline and during stimulation by isoproterenol (2 mg.kg^{-1} body weight) and caffeine (120 mg.kg^{-1} body weight). B] Quantification of WT and Pkp2-Het mice heart rates at baseline and during adrenergic stimulation. N= 6–7 hearts per group. Bpm: Beats per minute. C] Arrhythmias recorded in Pkp2-Het hearts after sympathetic stimulation. a) Monomorphic and b) polymorphic ventricular tachycardia, and c) ventricular fibrillation followed by atrio-ventricular block and cardiac arrest. D] Mouse susceptibility to arrhythmias during

ISO + caffeine stimulation. Left: Frequency of non-sustained arrhythmias (≤5 seconds); Right: Frequency of sustained arrhythmias (>5 seconds). E] Percentage of mice who died from arrythmias during the recordings. Notice how adrenergic stimulation exacerbated the sensitivity of Pkp2-Het hearts to arrhythmic events and premature death. N= 6–7 mice per group. F] Representative recordings of Ca^{2+} transients (1 Hz pacing) and caffeine-induced Ca^{2+} transients of LVFW cardiac myocytes, isolated from six-month-old WT and Pkp2-Het hearts, stimulated by 100 nM isoproterenol. G] Ca^{2+} transient amplitudes and H] Sarcoplasmic reticulum Ca^{2+} contents were significantly increased in LVFW myocytes from aging Pkp2-Het compared to those in age-matched WT myocytes. n= 21–33 cells per 3–4 hearts per group. *: $P<0.05$ and **: $P<0.01$ vs. age-matched WT. ***: $P<0.001$ vs. baseline.

Table 1:

Contraction properties of ventricular myocytes isolated from Pkp2-Het and WT hearts paced at 3 Hz at RT in 1.8 mM Ca^{2+} Tyrode's solution.

	3-month-old		6-month-old		12-month-old	
	WT	P2	WT	P2	WT	P2
N=	6	6	6	6	6	5
LVFW myocytes						
Total number of cells	21	20	23	29	22	22
Sarc. length base (μm)	1.79±0.01	1.78±0.01	1.79±0.01	1.78±0.01	1.77±0.01	1.79±0.01
Diastolic length (μm)	1.74±0.01	1.74±0.02	1.75±0.01	1.73±0.01	1.73±0.01	1.74±0.01
Peak length (μm)	1.54±0.02	1.56±0.02	1.54±0.01	1.50±0.01	1.53±0.02	1.55±0.02
Amplitude (%)	12.0±0.7	10.7±0.8	12.3±0.7	12.9±0.6	11.9±0.7	11.7±0.7
Contraction v. (-μm.s^{-1})	4.70±0.3	4.04±0.3	4.94±0.3	5.18±0.3	4.72±0.3	4.70±0.3
Relaxation v. (μm.s^{-1})	3.69±0.3	3.31±0.4	4.24±0.4	3.90±0.3	3.53±0.3	3.51±0.4
RVFW myocytes						
Total number of cells	26	24	25	21	23	25
Sarc. length base (μm)	1.78±0.01	1.79±0.01	1.76±0.01	1.78±0.01	1.78±0.01	1.76±0.01
Diastolic length (μm)	1.76±0.01	1.77±0.01	1.72±0.01	1.76±0.01	1.75±0.01	1.73±0.01
Peak length (μm)	1.57±0.01	1.60±0.01	1.54±0.02	1.62±0.01$^{\$}$	1.56±0.02	1.60±0.01
Amplitude (%)	10.58±0.7	9.17±0.6	10.59±0.7	8.15±0.5$^{\$\#}$	10.94±0.7	7.58±0.5$^{a\#}$
Contraction v. (-μm.s^{-1})	4.11±0.3	3.54±0.3	3.84±0.3	3.02±0.2$^{*\#}$	4.26±0.3	2.81±0.2$^{\$\#}$
Relaxation v. (μm.s^{-1})	3.15±0.3	2.52±0.2	2.78±0.3	2.25±0.2$^{\#}$	3.10±0.2	1.95±0.2$^{\$\#}$

Sarc. length base: Sarcomere length at diastole during 0.5 Hz pacing. Diastolic and peak lengths were measured at 3 Hz. V.: Velocity.

*: $P<0.05$,

$^{\$}$: $P<0.01$, and

^{a}: $P<0.001$ vs. age-matched WT myocytes.

$^{\#}$: $P<0.001$ vs. age-matched LV myocytes.

Table 2:

Ca^{2+} transient characteristics of Fura-2-loaded isolated ventricular myocytes paced at 1 Hz at RT in 1.8 mM Ca^{2+} Tyrode's solution.

	3-month-old		6-month-old		12-month-old	
	WT	P2	WT	P2	WT	P2
N=	5	6	6	6	6	5
LV myocytes						
Total number of cells	33	33	23	28	33	33
Diastolic $[Ca^{2+}]_i$ (Fura-2)	0.61±0.01	0.60±0.01	0.61±0.02	0.61±0.01	0.63±0.01	0.66±0.01
Peak $[Ca^{2+}]_i$ (Fura-2)	0.95±0.02	0.96±0.02	0.98±0.03	0.99±0.03	1.04±0.02	1.11±0.02
Δ $[Ca^{2+}]_i$ (Fura-2)	0.34±0.01	0.36±0.02	0.37±0.02	0.38±0.02	0.41±0.01	0.45±0.02
Time to peak (ms)	27.8±1.03	31.2±1.01	31.9±1.08	34.7±1.32	34.6±1.30	34.7±1.34
Tau (sec)	0.25±0.01	0.21±0.01	0.23±0.02	0.24±0.01	0.18±0.01	0.18±0.01
Δ caffeine (Fura-2)	0.50±0.02	0.51±0.02	0.52±0.03	0.52±0.02	0.54±0.02	0.57±0.02
Caffeine decay (sec)	2.25±0.14	2.28±0.16	2.77±0.36	3.04±0.22	2.88±0.20	2.69±0.19
Fractional Ca^{2+} rel. (%)	68.6±3.15	69.4±3.62	72.5±2.62	75.7±3.02	80.3±3.14	81.9±3.77
RV myocytes						
Total number of cells	30	39	19	28	29	30
Diastolic $[Ca^{2+}]_i$ (Fura-2)	0.61±0.01	0.62±0.01	0.65±0.02	0.64±0.01	0.65±0.01	0.67±0.01
Peak $[Ca^{2+}]_i$ (Fura-2)	0.86±0.02	0.91±0.02	0.93±0.02	0.95±0.03	0.98±0.02	0.99±0.03
Δ $[Ca^{2+}]_i$ (Fura-2)	0.25±0.01*	0.29±0.01*	0.28±0.02*	0.31±0.02*	0.33±0.02*	0.32±0.02*
Time to peak (ms)	25.3±1.32	24.0±0.61*	28.5±1.70	29.7±1.21*	30.3±1.74*	26.1±1.07*
Tau (sec)	0.33±0.01*	0.29±0.02*	0.31±0.02*	0.30±0.02*	0.23±0.02*	0.28±0.02*
Δ caffeine (Fura-2)	0.47±0.02	0.51±0.02	0.49±0.02	0.50±0.03	0.51±0.02	0.56±0.02
Caffeine decay (sec)	2.16±0.13	2.47±0.16	3.09±0.22	3.30±0.67	3.15±0.30	2.58±0.15
Fractional Ca^{2+} rel. (%)	54.4±2.20*	56.9±2.12*	55.8±4.08*	58.8±2.63*	64.8±3.10*	58.4±4.26*

Δcaffeine: (10 mM) caffeine-induced Ca^{2+} transient amplitude; Fractional Ca^{2+} rel.: Fractional Ca^{2+} release; Fura-2: Fura-2 ratio 340nm/380nm.

*: $P<0.05$ vs. age-matched LV myocytes.